Mineral Economics (2022) 35:495–502
https://doi.org/10.1007/s13563-022-00327-1

COMMENT

Implications of new hyperspectral satellites for raw materials exploration

Martin C. Schodlok[1] · **Michaela Frei**[1] · **Karl Segl**[2]

Received: 1 March 2022 / Accepted: 26 May 2022 / Published online: 27 June 2022
© The Author(s) 2022

Abstract

Hyperspectral remote sensing already is important in geoscientific research in the fields of geology, soil, exploration and mining. New hyperspectral satellite systems are already in operation (e.g. PRISMA and DESIS; Caporusso et al. 2020; Alonso et al. (Sensors 19(20):4471–4515, 2019)) and more systems are planned e.g. the European Copernicus Next Generation Hyperspectral Satellite CHIME (Nieke and Rast 2018). The German system EnMAP was successfully launched into space on 1st of April 2022 (DLR 2022). The potential of hyperspectral airborne and satellite borne data for mining-related applications is discussed. Investigated are the information contents of hyperspectral data for exploration target recognition and their dependency on spatial resolutions of different sensor platforms. Airborne data offer high spatial resolution of 2.5 m with limited areal data acquisition, whereas hyperspectral spaceborne sensors guaranty nearly worldwide data availability with the same spectral characteristics but medium spatial resolution (30 m). The aspects of high spectral resolution and high versus medium spatial resolution targeted mineral mapping is investigated. The methodological concept includes processing aspects, standardized data availability for mineral mapping and mineralization targeting for operational application, to maintain/allow application of hyperspectral data even for non-remote sensing experts. Based on hyperspectral airborne data acquired in the Aggeneys region in South Africa, spaceborne hyperspectral data are simulated following the EnMAP specifications, and the concept for targeted mapping of surface alterations of a lead zinc deposit is discussed.

Keywords Exploration · Mineral mapping · Hyperspectral imaging · EnMAP · VNIR-SWIR

Introduction

In geological applications hyperspectral imaging using the visible light, the near infrared (VNIR) and the shortwave infrared (SWIR) wavelength range from 0.4 to 2.5 µm is a well-known technique to discriminate lithology due to their mineral diagnostic spectral features and to derive mineral maps. In this given wavelength range, minerals such as hydroxyl bearing silicates, sulfates, phosphates, borates, carbonates and hydroxides can be identified (Hunt 1970, 1971; Hunt et al. 1972; Hunt and Salisbury 1971). Many studies have already demonstrated this potential by using data acquired by airborne, terrestrial or laboratory sensor systems (e.g. Kruse 2012; van der Meer et al. 2012; van Ruitenbeek et al. 2019). These sensors provide information from local to regional scale, depending on availability of the systems as well as trained operators for the acquisition of high quality data. With new satellite systems such as PRISMA launched in 2019 (Caporusso et al. 2020), EnMAP (Guanter et al. 2015) or CHIME (Nieke and Rast 2018), a European Copernicus Satellite scheduled for launch in launched April 2022 2025 + hyperspectral data with a regional to global scale are provided or will soon be available from space. This new context also increases the availability of hyperspectral data at lower costs compared to airborne acquisitions since the above-mentioned satellite systems follow an open access data policy. Therefore, it allows the remote sensing community to develop new products, which can support the mining industry for cost effective exploration activities by delivering e.g. mineral maps of

✉ Michaela Frei
Michaela.Frei@bgr.de

[1] Subdivision Remote Sensing, Federal Institute for Geosciences and Natural Resources (BGR), Hannover, Germany

[2] Section 1.4: Remote Sensing and Geoinformatics, Helmholtz-Centre Potsdam - GFZ German Research Centre for Geosciences, Potsdam, Germany

large areas or mineral detection products (alteration zone maps, mineral vector maps) for targeted exploration. This study aims at assessing the potential of hyperspectral data to support exploration activities at different scales — from Satellite — to airborne. Therefore, hyperspectral airborne and satellite data are applied to map the lithostratigrafic units connected to lead–zinc-copper mineralization zones of Aggeneys in the Northern Cape Province of South Africa (Fig. 1). It emphasises on the differentiation of the major mineralogy as well as the detection of a gossan as indicator for the Gamsberg zinc mineralization. Validation is performed based on geological maps and ground truth data.

Geological setting

Gamsberg is an inselberg as part of the Aggeneys area located in the northwest of the Northern Cape region of South Africa. It is about 7 km long, 5 km across and steep sided with an elevation of 1150 m above sea level and 250 m above the plain ground.

The Mesoproterozoic Aggeneys-Gamsberg ore district hosts one of the world's largest sulfidic base metal complex, classified as a Broken Hill-type base metal deposit which are traditionally interpreted as metamorphosed sedimentary exhalative (SEDEX) deposits (Höhn et al. 2021b; Rozendaal et al. 2017; Stalder and Rozendaal 2005). Recent investigations support the hypothesis that the massive sulfide deposits in the Aggeneys district show a more complex history, after initial SEDEX-type mineralization near–surface oxidation and sulfidation of the oxidized ore during medium- to high-grade metamorphism took place (Willner et al. 1990; Höhn et al. 2021a).

The Gamsberg deposit is part of the western area of the Namaqua-Natal Province. Stratigraphically, the ore units are part of a volcano-sedimentary succession (Bushmanland Group, Fig. 1). The main lithological units of Gamsberg consist of metasediments with intercalated base metal mineralizations, metavolcanics and metagneisses. The lithologies range from biotite-sillimanite schist, paragneiss, quartzite, in places graphite-rich sillimanite-mica, schist, and at the top of the group, especially in the vicinity of the stratiform ore bodies, meta-exhalites like iron formation. The deposition age of the base metal-rich strata is constrained between 1285 ± 14 and 1198 ± 10 Ma (Cornell et al. 2009). The ore mineralization at the top of the Hoston Formation is characterized by psammo-pelitic shists at the base and the top and the ore zone in between (also known as Gams Member, Stalder and Rozendaal 2004). Gamsberg deposit hosts a strongly Zn-dominated ore, followed by lead and copper. During field work, the surface expressions of the

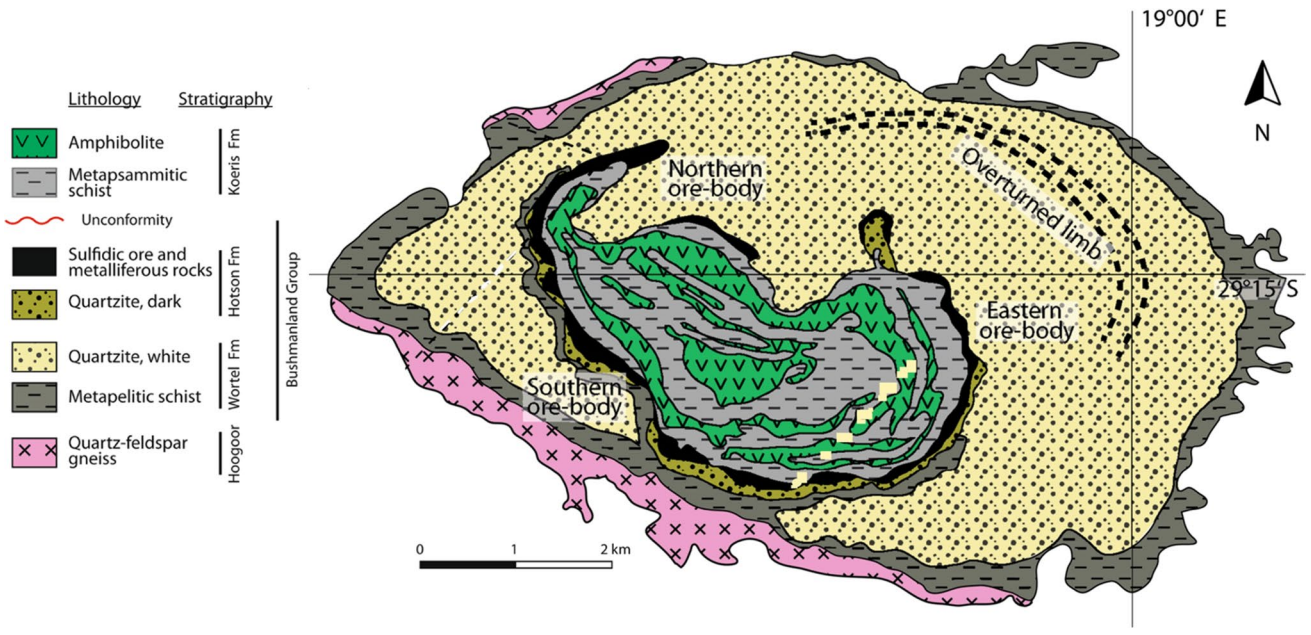

Fig. 1 Geological situation of the Gamsberg deposit (after Stalder and Rozendaal 2004 and Höhn et al. 2021a, b)

ore body are found at Gamsberg as gossan dominated by hematite which was confirmed by personal communication with Potti Potgieternd (2015). The Bushmanland Group is unconformably overlain by the Kories Formation (volcano-sedimentary).

Multiscale data sources concept

Airborne data

The Gamsberg airborne hyperspectral data set consists of 18 flight lines acquired during a campaign in South Africa in July/August 2015 by two sensors (Hyspex VNIR 1600 and SWIR 320me systems from NEO, Norway) covering the visible light, the near Infrared and the shortwave infrared wavelength range (VNIR-SWIR) from 400 to 2500 nm. The hyperspectral data acquired have a ground sampling distance of 2.5 m and in addition, LIDAR data are acquired to create surface and terrain models with a spatial resolution of 1 m. For further application assessment, the hyperspectral data have been radiometrically corrected, orthorectified using ground control points and the software package PARGE. The atmospheric correction based on the Airborne Atmospheric and Topographic Correction Model (ATCOR4) has been applied to derive surface reflectance values. Since two sensors are used to collect the data, the two data streams are co-registered and layerstacked to build a single VNIR-SWIR data cube per flight line. Finally, the data cubes mosaicked to a single data set (Fig. 2A). Further pre-processing steps include the calculation of shadow and vegetation masks. For the shadow mask all pixel with reflectance values less than 5% are marked as shadow and for the vegetation mask an NDVI approach is applied with a defined threshold of 0.4.

Satellite data

Hyperspectral satellite EnMAP data are simulated based on the hyperspectral airborne data set. EnMAP stands for the **En**vironmental **M**apping and **A**nalysis **P**rogram and is a German hyperspectral satellite mission that aims at monitoring and characterizing the Earth's environment on a global scale. The satellite is launched on April 1st, 2022 (DLR 2022) . The satellite includes an imaging pushbroom system covering with two sensors the wavelength range from 420 to 2450 nm (VNIR-SWIR) and provides a spatial resolution of 30 m × 30 m and a swath of 30 km. The spectral resolution is 6.5 nm for the VNIR sensor and 10 nm for the SWIR sensor compared to the spectral resolution of the Hyspex systems of 3.7 nm for the VNIR and 6 nm for the SWIR. The target signal to noise ratio (SNR) is 4001:1 at 495 nm and 170:1 at 2200 nm.

As part of the system's development, the EnMAP End-to-End Simulation tool (EeteS) developed at GFZ (Segl et al. 2010, 2012) provides accurate simulation of the entire image generation, calibration and processing chain as well as realistic image products generation to scientists in advance. The HySpex surface reflectance data are the input to generate an EnMAP-simulation image of the Aggeneys area.

The HySpex data conversion into raw EnMAP data used in the beginning a series of forward processing steps including modelling of the spaceborne versus airborne atmospheric conditions and account for the spatial, spectral, and radiometric characteristics of VNIR and SWIR EnMAP sensors. Then, the software simulates the entire EnMAP image processing chain from raw to radiometric calibrated data. Finally, the spatial correction is performed, where the data are transformed into the UTM reference grid and atmospherically corrected. Figure 2A and 2B show the

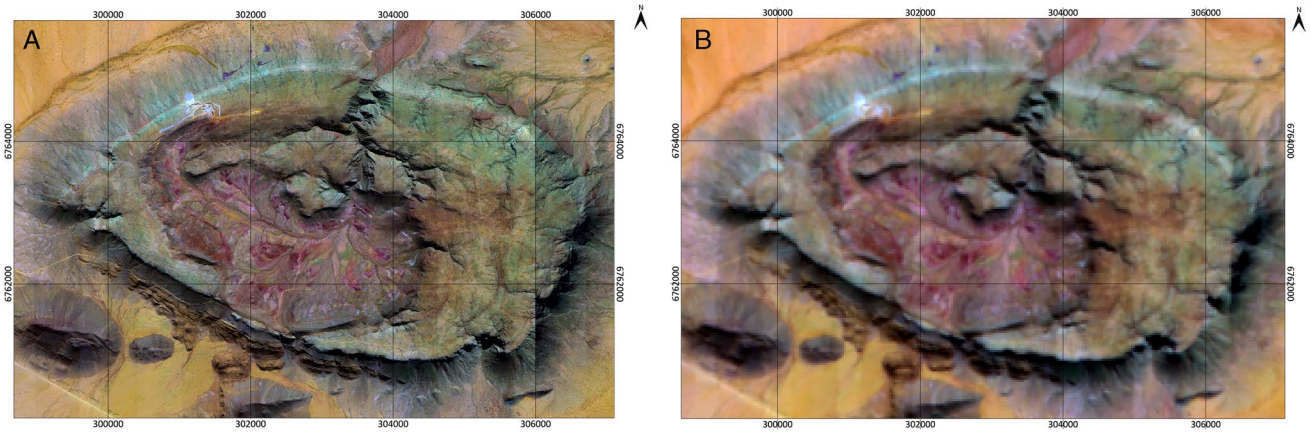

Fig. 2 False colour composite of Gamsberg using the wavelengths 2204, 900 and 470 nm RGB coded. (**A**) Hyspex data and (**B**) simulated EnMAP data

original hyperspectral airborne data on the right (2.5 m spatial resolution) and the simulated EnMAP data (30 m spatial resolution) on the left as false colour composite using the wavelength of 470, 900 and 2204 nm for the RGB coding.

Field and laboratory spectroscopy

During the flight campaign, a comprehensive field campaign has been carried out for calibration and validation purposes. Therefore, field spectra are acquired using an ASD Field Spec HR4. The calibration and validation targets with a size of approx. 10 × 10 m have been sampled, each with 20–30 single measurements to assess their spectral characteristics following the protocol recommended by CSIRO (Malthus et al. 2019). The field spectra of the calibration targets are included in the atmospheric correction procedure for the airborne hyperspectral data. For validation purposes, approx. 30 rock and soil samples have been collected from Aggeneys area for further laboratory spectral measurements using an Analytical Spectral device (ASD) fieldspec HR4. These laboratory spectra are added to the mineral spectral database. Additionally, geochemical and mineralogical analyses are applied on the samples by XRF using a Zetium Panalytical device and XRD using a PANalytical MPD Pro device, respectively.

Methodology

For mineral mapping, the spectral feature fitting (SFF) approach included in software package ENVI (2022) is applied. This approach compares mineral diagnostic spectral absorption features (grey indicated areas) from reference minerals (Fig. 3A) with spectral features of the image pixel spectra (Fig. 3B) based on a least-square technique. In this approach, five respective minerals are identified for the mineral mapping. Thus, reference mineral spectra from muscovite, illite, kaolinite, hornblende and hematite selected from the USGS spectral library (Kokaly et al. 2017) are resampled to the spectral resolution of the airborne hyperspectral image data. The wavelength interval relevant for muscovite spectral characterization is between 2010 and 2240 nm, for Illite between 2156 and 2276 nm, for kaolinite between 2132 and 2228 nm, hornblende between 2252 and 2468 nm and for hematite, two wavelength intervals at 630–1200 nm and 2126–2234 nm are defined. The second interval for clear hematite recognition is necessary to separate hematite from other Fe-bearing minerals e.g. amphiboles, showing their diagnostic feature in the SWIR wavelength at ~ 2320 nm whereas hematite does not (Fig. 3). The SSF approach generates an image where large values represent a good fit between reference and image data and low numbers a bad or no fit. Followed by that, the image is post classified by applying thresholds available in Tables 1 and 2 for the best fit. First, a percent clip of max 5% of the SFF result defined the thresholds as a starting point. In a second step, the threshold values were adjusted by visual interpretation to assure misclassifications.

Results and discussion

Figure 4 shows the classification result of the airborne HySPEX (Fig. 4A) and the simulated spaceborne EnMAP data (Fig. 4B), respectively — colour coded to muscovite (turkise), illite (dark turkise), kaolinite (blue and light blue), hematite (red) and hornblende representing

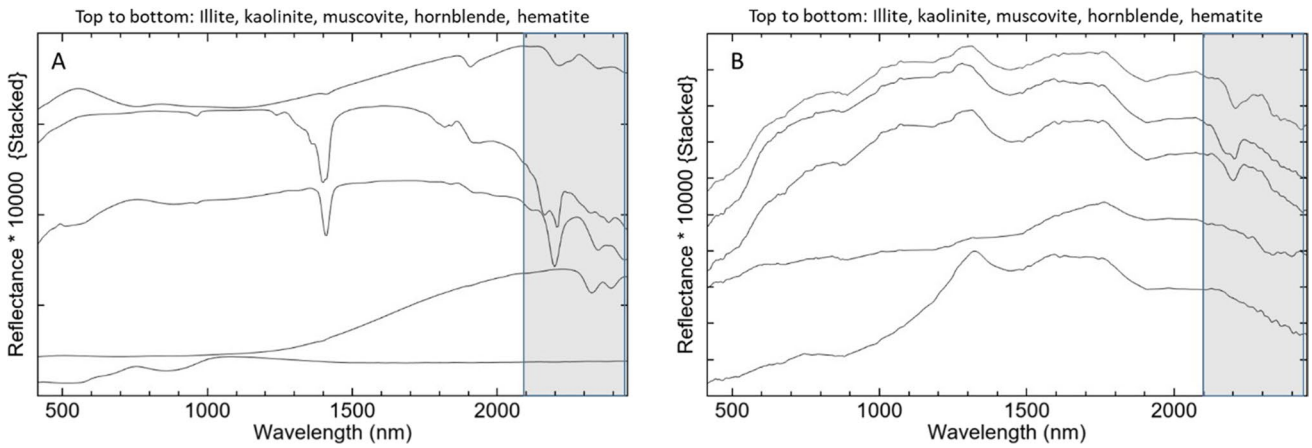

Fig. 3 (**A**) Example reference spectra of muscovite, illite and kaolinite from the USGS spectral library v7 (Kokaly et al. 2017) in comparison with (**B**) airborne hyperspectral image pixel spectra of the same minerals

Table 1 Parameters of classification for the spectral feature intervals and thresholds of airborne HySpex data

	Spectral feature		Classification
Mineral	Start (nm)	End (nm)	Threshold interval
Illite	2156	2276	40–131
Muscovite	2110	2240	200–330
Kaolinite WX	2132	2228	18–40
Kaolinite PX	2132	2228	150–375
Amphibole	2252	2468	17–38
FE anomaly	630	1200	12–18
Hematite	630	1200	0.01–0.14
	2126	2234	

the mineral group of amphiboles (purple). In addition to the five mineral endmembers, a further endmember was identified, not related to a given mineral. The additional endmember is an indicator for a significant higher amount of iron content in a pixel and identifies areas with an enrichment of iron — so called 'Fe anomaly' (yellow). This 'Fe-anomaly' can be described as spectral expression or mixture of spectral signals from hematite and iron-enriched minerals such as micas, amphiboles and others, not to be distinguished based on the hyperspectral data investigated. The spatial resolution of 2.5 m per pixel results in so-called mixspectra, which expresses the sum of the aerial fractions of the above-mentioned classes; thus, it is difficult to distinguish spectrally between these minerals and native iron. Therefore, areas with an enrichment in iron is pointed out as an own classification unit 'Fe anomaly'. Both images show very similar distribution patterns of the detected minerals and of 'Fe' distribution pattern, which follow the major lithological units from the geological map (Fig. 1). Kaolinite and muscovite are associated to the quartzites and minor within the schists, illite represents the majority of the schists as their main mineral phase, hornblende indicates the amphibolites and hematite is an indicator for gossans as surface expression of the ore mineralization. The quartzites separate into two major domains, where the kaolinite dominates the northeastern area of the quartzites and muscovite the southwestern region. Within the kaolinite classification, a separation between well crystalline (wx) and poor crystalline (px) kaolinite is achieved but only visible for the airborne data. The poor crystalline type is characterized by the lack of the absorption feature at ~ 2163 nm of the known double feature of kaolinite in the SWIR range (Fig. 3) (Cudahy 1997). Due to lower spectral resolution of the simulated EnMAP data (Fig. 5), this clear differentiation for the kaolinite phases in airborne data is not achieved for the satellite data. The lower spectral resolution of the satellite data leads to loss of the first kaolinite feature at ~ 2163 nm of the kaolinite double feature. Illite and amphiboles are present in the centre of Gamsberg, which is in good agreement with the geological map (Fig. 1). The 'Fe' anomaly indicates the Gams Member/Hoston F., which hosts the mineralization of Gamsberg, this result is in full agreement with the geological map. A few 'Fe' anomaly spots in addition appear in the south of Gamsberg, which are assumed to be related to an increase of 'Fe' content in the muscovite of the white quartzites and pelitic schist of the Wortel Fm. of the Bushmannland Group (Fig. 1). The simulated EnMAP image shows a similar pattern of the Fe anomaly along the Gams Member. In contrast to the HySpex data, the spatial distribution is larger and in addition, large patches are present at the inner eastern rim of Gamsberg, as well as larger patches in the south of Gamsberg. This might be caused by the different spatial ground resolution of the simulated satellite imagery (30 m) compared to the airborne data (2.5 m) resulting in larger spectral mixtures per pixel. This leads to the assumption that the 'Fe' proportion and therefore its spectral signature, dominates the spectral mixture over other minerals signatures in the larger pixel of the satellite imagery compared to the smaller pixel of the airborne imagery leading to this result.

Table 2 Parameters of classification for the spectral feature intervals and thresholds of simulated EnMap data

	Spectral feature		Classification
Mineral	Start (nm)	End (nm)	Threshold interval
Illite	2167	2267	40–75
Muscovite	2141	2267	65–110
Kaolinite	2132	2237	17–40
Amphibole	2267	2430	33–80
FE anomaly	670	1000	27–100
Hematite	670	1000	0.01–0.07
	2079	2307	

However, in the satellite imagery, the hematite is clearly identified. It follows the same distribution as the Sulfidic ore and metalliferous rocks unit of the Hoston Formation in the geological map, and the two areas in the southwest (Fig. 4A and 4B zoom) are confirmed as outcropping gossans through fieldwork in 2015. As earlier mentioned, the gossan at Gamsberg consists dominantly of hematite. Therefore, hematite is used as the major proxy for the lead zinc mineralization of Gamsberg and is labelled as gossan in the classification result for better understanding. There is a fair amount of unclassified

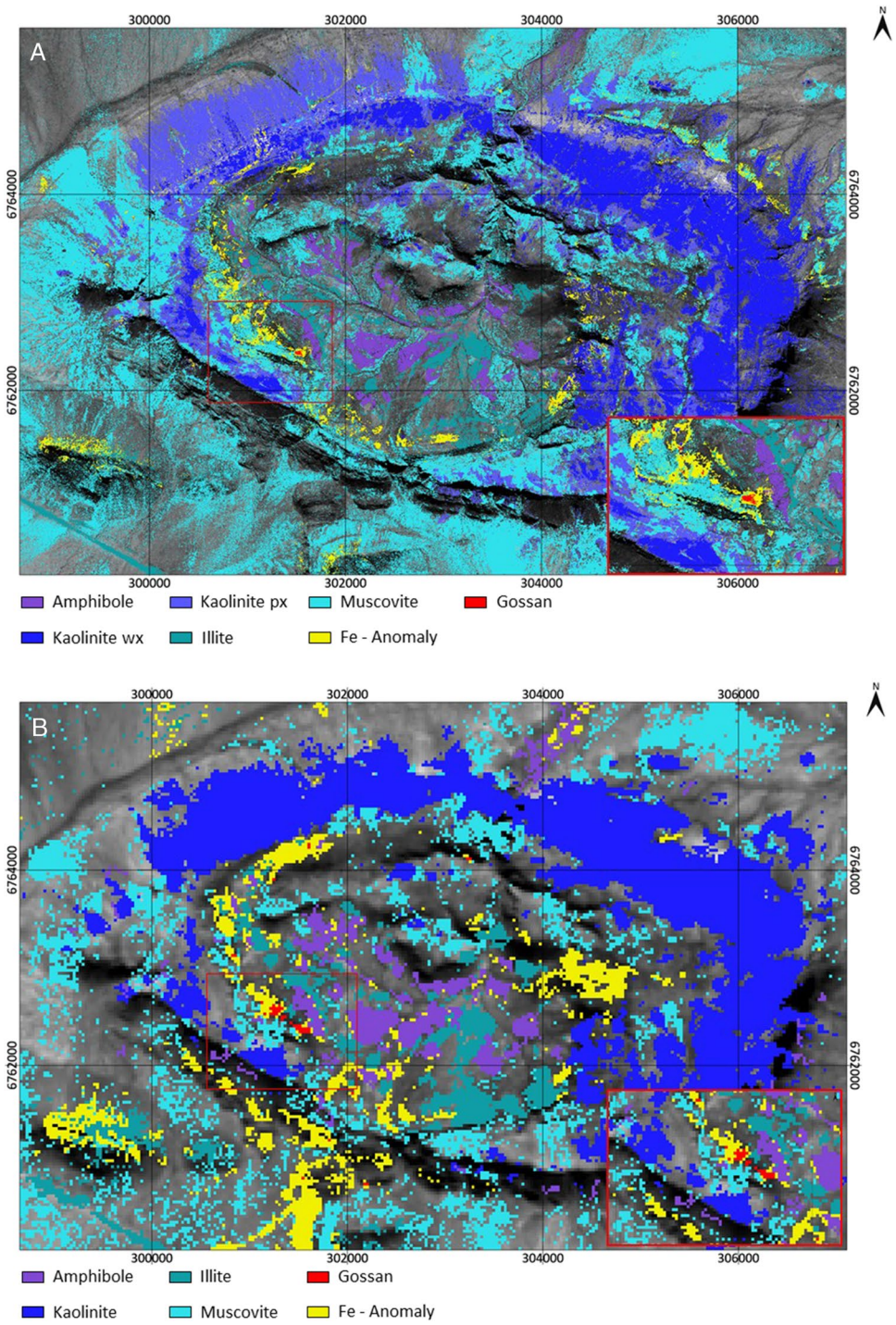

Fig. 4 (**A**) Mineral classifications of the airborne HySpex data and (**B**) of the simulated EnMAP data

pixel in the classification result. This relates to the large natural variation of spectral signatures of minerals dependent on variations in chemical compositions, and impurities and the physical condition of minerals affected by weathering. In addition, the mix of spectral signatures related to mineral assemblages in the rocks within a given pixel cannot fully be addressed by using pure individual reference mineral spectra for a classification and can lead to rejected pixel. Further reasons for the not classified pixel might be the conservative applied threshold definition to avoid misclassifications. The authors think that despite the unclassified pixel, the

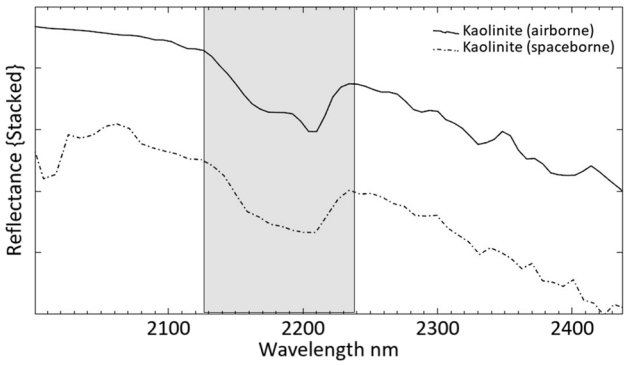

Fig. 5 Comparison of the spectral resolution of the airborne system (solid) and the simulated spaceborne data (dash dotted) using the example of a kaolinite spectrum. The grey-marked area indicates the kaolinite absorption feature

activities with three open pits with active ore excavations at Gamsberg, shown by a recent Sentinel 2 satellite imagery (Fig. 6). Two of these open pits are in the areas where the hematite is mapped by hyperspectral data as proxy for the Gossan. Since the simulated hyperspectral satellite imagery shows similar mineral pattern compared to the high spatial resolution imagery of the hyperspectral flight campaign, it indicates, that hyperspectral satellite data are an important data source for exploration activities despite the moderate spatial resolution. However, for detailed mapping especially within a mineralization zone, hyperspectral high spatial resolution data from airborne or unmanned aerial vehicle (UAV) systems are important, to understand and to map the mineralogy of such a zone in their complete complexity.

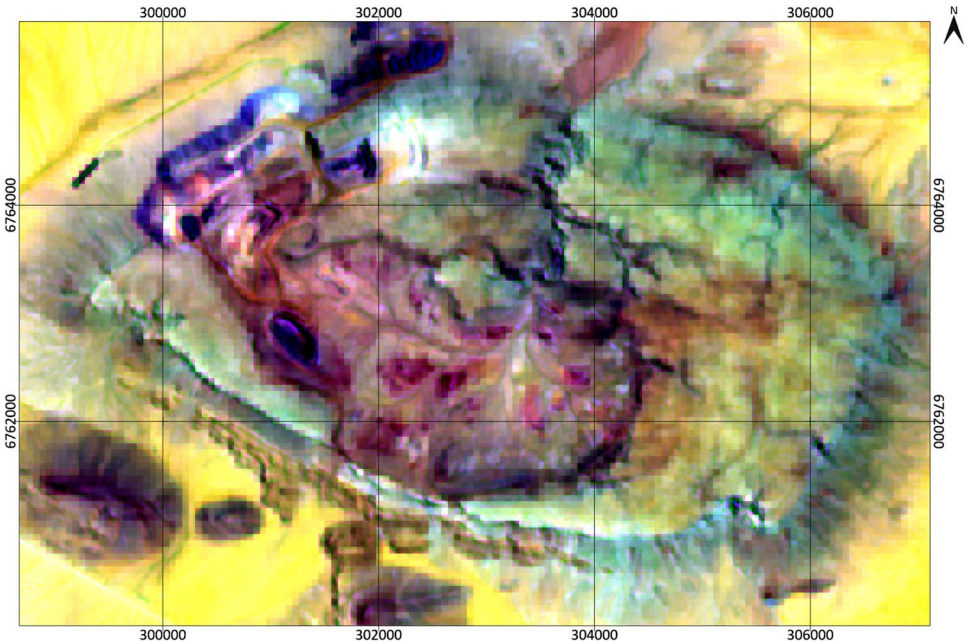

Fig. 6 ESA Copernicus Sentinel 2 (Szantoi and Strobl 2019) image from 19.12.2021 as false colour composite (RGB: B12,8a,2) showing the current mining activities in blue to purple colour, locations are in agreement with the 'Fe' anomaly and Gossan (hematite) classification from Fig. 4A and 4B

classification result reflects the distribution of the major mineralogy as well as shows that hyperspectral satellite data can detect potential ore mineralization, in this case by identifying the gossan.

Conclusion

This study shows that simulated hyperspectral satellite data are analyzed successfully to map major mineralogy and proxy minerals for the ore mineralization at Gamsberg. It is possible clearly to detect the Gossan (hematite distribution) as surface expression of the lead zinc mineralization. This is in good agreement by current mining

Acknowledgements We gratefully thank VEDANTA Zinc International (VUI) and Black Mountain Mining (PTY) LTD for the support and access to Gamsberg and their facilities of the Aggeneys ore field. We also want to thank Markus Schaefer, Jaco Smit from VZI for providing geological information and rock samples as well all the fruitful discussion, and further we thank Pottie Potgieternd and Pieter Gene Steinmann from VZI Black Mountain Mining for their engagement and their support during the fieldwork at Gamsberg/Aggeneys.

Author contribution All authors have worked on the manuscript equally.

Funding Open Access funding enabled and organized by Projekt DEAL. Funding provided by BGR.

Data availability Data available at BGR for selected applications.

Code availability Not applicable.

Declarations

Conflict of interest The authors declare no competing interests.

Open Access This article is licensed under a Creative Commons Attribution 4.0 International License, which permits use, sharing, adaptation, distribution and reproduction in any medium or format, as long as you give appropriate credit to the original author(s) and the source, provide a link to the Creative Commons licence, and indicate if changes were made. The images or other third party material in this article are included in the article's Creative Commons licence, unless indicated otherwise in a credit line to the material. If material is not included in the article's Creative Commons licence and your intended use is not permitted by statutory regulation or exceeds the permitted use, you will need to obtain permission directly from the copyright holder. To view a copy of this licence, visit http://creativecommons.org/licenses/by/4.0/.

References

Alonso K, Bachmann M, Burch K, Carmona E, Cerra D, de los Reyes R et al (2019) Data products, quality and validation of the DLR earth sensing imaging spectrometer (DESIS). Sensors 19(20):4471–4515. https://doi.org/10.3390/s19204471 (Multidisciplinary Digital Publishing Institute (MDPI))

Caporusso G, Lopinto E, Lorusso R, Loizzo R, Guarini R, Daraio MG et al (2020) The hyperspectral PRISMA mission in operations. IEEE IGARSS 2020 Proceedings. 3282–3285

Cornell DH, Pettersson A, Whitehouse MJ, Schersten A (2009) A new chronostratigraphic paradigm for the age and tectonic history of the Mesoproterozoic Bushmanland ore district, South Africa; reply. Econ Geol Bull Soc Econ Geol 104(8):1282–1285. https://doi.org/10.2113/gsecongeo.104.8.1282

Cudahy TJ (1997) PIMA-II Spectral Characteristics of Natural Kaolins. CSIRO Exploration and Mining Report 420R. Commonwealth Scientific and Industrial Research Organisation (CSIRO), Canberra

DLR (2022) German satellite EnMAP launches successfully. DLR News - 01.04.2022. https://www.dlr.de/content/en/articles/news/2022/02/20220401_german-satellite-enmap-launches-successfully.html. Accessed 18 April 2022

ENVI (2022) https://www.l3harrisgeospatial.com/Software-Technology/ENVI

Guanter L, Kaufmann H, Segl K, Foerster S, Rogass C, Chabrillat S et al (2015) The EnMAP spaceborne imaging spectroscopy mission for earth observation. Remote Sens 7:8830–8857. https://doi.org/10.3390/rs70708830

Höhn S, Frimmel HE, Price W (2021a) Syn-metamorphic sulfidation of the Gamsberg zinc deposit, South Africa. Mineral Petrol 115:709–728. https://doi.org/10.1007/s00710-021-00764-w

Höhn S, Frimmel HE, Debaille V, Price W (2021b) Pre-Klondikean oxidation prepared the ground for Broken Hill-type mineralization in South Africa. Terra Nova 33:168–173. https://doi.org/10.1111/ter.12502

Hunt GR (1970) Visible and near-infrared spectra of minerals and rocks: I silicate minerals. Mod Geol 1:283–300

Hunt GR (1971) Visible and near-infrared spectra of minerals and rocks: III. oxides and hydro-oxides. Mod Geol 2:195–205

Hunt GR, Salisbury JW (1971) Visible and near infrared spectra of minerals and rocks. II. Carbonates Mod Geol 2:23–30

Hunt GR, Salisbury JW, Lenhoff CJ (1972) Visible and near infrared spectra of minerals and rocks: V. halides, phosphates, arsenates, vanadates and borates. Mod Geol 3:121–132

Kokaly RF, Clark RN, Swayze GA, Livo KE, Hoefen TM, Pearson NC, Wise RA, Benzel WM, Lowers HA, Driscoll RL, Klein AJ (2017) USGS Spectral Library Version 7 Data Series. Reston, VA, p 68

Kruse FA (2012) Mapping surface mineralogy using imaging spectrometry. Geomorphology 137(1):41–56. https://doi.org/10.1016/j.geomorph.2010.09.032

Malthus TJ, Ong C, Lau I, Fearns P, Byrne G, Thankappan M et al (2019) A community approach to the standardised validation of surface reflectance data. A technical handbook to support the collection of field reflectance data. Release version 1.0. CSIRO. Australia. ISBN: 978–1–4863–0991–7

Nieke J, Rast M (2018) Towards the Copernicus hyperspectral imaging mission for the environment (CHIME). IGARSS 2018 - IEEE Int Geosci Remote Sens Symp 157–159. https://doi.org/10.1109/IGARSS.2018.8518384

Rozendaal A, Rudnick TK, Heyn R (2017) Namaqua sector of the Namaqua-Natal Metamorphic Province, South Africa: a review. S Afr J Geol 120(1):153–186. https://doi.org/10.25131/gssajg.120.1.153

Segl K, Guanter L, Kaufmann H (2010) Simulation of spatial sensor characteristics in the context of the EnMAP hyperspectral mission. IEEE Trans Geosci Remote Sens 48:3046–3054

Segl K, Guanter L, Kuester T, Roessner R, Kaufmann H, Sang B (2012) EeteS - The EnMAP end-to-end simulation tool. IEEE J Sel Top Appl Earth Obs Remote Sens 5:522–530

Stalder M, Rozendaal A (2004) Apatite nodules as an indicator of depositional environment and ore genesis for the Mesoproterozoic Broken Hill-type Gamsberg Zn–Pb deposit Namaqua Province, South Africa. Miner Deposita 39:89–203. https://doi.org/10.1007/s00126-003-0394-8

Stalder M, Rozendaal A (2005) Distribution and geochemical characteristics of barite and barium-rich rocks associated with the broken hill-type Gamsberg Zn-Pb deposit, Namaqua Province, South Africa. S Afr J Geol 108(1): 35-50. https://doi.org/10.2113/108.1.35

Szantoi Z, Strobl P (2019) Copernicus sentinel-2 calibration and validation. Eur J Remote Sens 52:253. https://doi.org/10.1080/22797254.2019.1582840

Van der Meer FD, Van der Werff HMA, Van Ruitenbeek FJA, Hecker CA, Bakker WH, Noomen MF et al (2012) Multi - and hyperspectral geologic remote sensing: a review. Int J Appl Earth Obs Geoinf 14(1):112–128. https://doi.org/10.1016/j.jag.2011.08.002

Van Ruitenbeek FJA, van der Werff HMA, Bakker WH, van der Meer FD, Hein KAA (2019) Measuring rock microstructure in hyperspectral mineral maps. Remote Sens Environ 220:94–109. https://doi.org/10.1016/j.rse.2018.10.030

Willner A, Schreyer W, Moore JM (1990) Peraluminous metamorphic rocks from the Namaqualand metamorphic complex (South Africa); geochemical evidence for an exhalation-related, sedimentary origin in a mid-Proterozoic rift system. Chem Geol 81(3):221–240. https://doi.org/10.1016/0009-2541(90)90117-P

Publisher's note Springer Nature remains neutral with regard to jurisdictional claims in published maps and institutional affiliations.